Fermi National Accelerator Laboratory

FERMILAB-Pub-83/30-EXP
7180.236
(Submitted to Nucl. Phys. B.)

A MEASUREMENT OF HIGH-P_T CORRELATIONS IN 340-GeV/c pp AND 280-GeV/c π^-p REACTIONS

W. P. Oliver
Tufts University, Medford, Massachusetts 02155

and

P. Limon, P. Mantsch, J. R. Orr, and S. Pruss
Fermi National Accelerator Laboratory, Batavia, Illinois 60510

and

V. Cook, G. Hicks, P. M. Mockett, J. E. Rothberg,
R. W. Williams, and K. K. Young
University of Washington, Seattle, Washington 98195

March 1983

A MEASUREMENT OF HIGH-P_T CORRELATIONS IN 340-GeV/c pp AND 280-GeV/c π^-p REACTIONS

W.P. OLIVER
Tufts University, Medford, Massachusetts 02155, USA

P. LIMON, P. MANTSCH, J.R. ORR and S. PRUSS
Fermilab, Batavia, Illinois 60510, USA

V. COOK, G. HICKS[1], P.M. MOCKETT, J.E. ROTHBERG,
R.W. WILLIAMS and K.K. YOUNG
University of Washington, Seattle, Washington 98195, USA

We have measured correlations between single high-p_T ($1.5<p_T<3.5$ GeV/c) trigger particles on one side of the beam line and groups of particles entering a calorimeter on the opposite side of the beam line. The mean transverse momentum measured in the calorimeter is found to increase with the trigger-particle transverse momentum. The coplanarity of the events increases with trigger-particle transverse momentum. We have compared our data to the predictions of a phenomenological four-jet model. To fit our data we find that we must give large (0.9 GeV/c) mean transverse momenta to the constituents of the initial hadrons.

1 Now at Bell Laboratories, Crawford-Corner Road, Holmdel, N.J. 07733, USA

I. INTRODUCTION

The possibility that large-momentum-transfer hadronic reactions might display a multiple jet structure and thereby reveal the nature of the interaction between the hadron constituents [1] has stirred experimentalists to undertake the types of difficult experiments required to study these rare processes.

Experiments to date have utilized calorimeters to achieve sensitivity to all hadrons in the jets. Calorimeters have the additional advantage of providing a prompt, relatively fool-proof p_T signal which can be used to trigger the apparatus. Our experiment is a member of the first group [2,3,4] of high-p_T-triggered large-acceptance experiments carried out at Fermilab. Subsequent experiments at CERN [5] and Fermilab [6] have used even larger-acceptance calorimeters to obtain a more complete view of the high-p_T reactions.

In addition to a calorimeter trigger, our experiment had the feature of being triggerable by a single high-p_T particle. The analysis of this feature of the experiment constitutes the present paper.

II. GENERAL PLAN OF THE EXPERIMENT

The experiment consisted of two large-aperture arms. The arms were orientated approximately back-to-back in the center-of-mass frame of the colliding beam and target particles. One arm was a 1.0-steradian-acceptance single-magnet spectrometer. The other arm was a 2.3-steradian-acceptance calorimeter. A plan view of the experiment is shown in Fig. 1. A beam view (in the center-of-mass frame for an incident 280-GeV/c π^-) is shown in Fig. 2. Our choice of coordinate system is defined in Figs. 1 and 2.

The plan of the experiment had two aspects. The experiment was designed to be triggered on either: (1) a high-p_t (> 2 GeV/c) charged particle in the spectrometer arm or (2) the collective transverse momentum possessed by a group of particles which happen to enter the calorimeter.

In the event of a spectrometer-arm trigger, the calorimeter arm served as an efficient detector of particles which may be recoiling from the trigger particle. The azimuthal acceptance of the calorimeter arm was made especially large to provide a wide field of view in which to search for a signal of particles which are coplanar with the trigger particle. Such a coplanarity signal would seem to result naturally in reactions which are dominated by a single hard-scattering process among the hadron constituents.

The calorimeter-trigger events served as a measurement of the probability that a group of particles within a restricted solid-angle will carry a large (> 2 GeV/c) transverse momentum. The distribution of particles within our large calorimeter in these high-p_t events can be analyzed for evidence of jet-like behavior.

We wanted to compare high-p_t reactions for both pion and proton beams. We further wanted to look for systematic variations in the number and form of high-p_t reactions with incident beam momentum.

The experiment was set up in the M1 beam line in the Meson Lab at Fermilab.

Data were taken for positively charged beam particles at momenta of 100, 200 and 340 GeV/c. Data for negative beam particles were taken at momenta of 100, 200 and 280 GeV/c.

An analysis of the calorimeter-triggered data for 100, 200 and 340 GeV/c pp reactions has been previously reported [4]. In this paper we concentrate on the analysis of spectrometer-triggered data at our highest beam energies.

III. APPARATUS

A. The Beam and Target

Particles for our beam were produced by collisions of 400-GeV/c-momentum protons with the Meson Lab target. The M1 beam line accepts particles produced at 3.5 mrad. The particles were transmitted a distance of 430 meters to our experimental area. We took data for positive-beam intensities ranging from 2×10^6/sec at 100 GeV/c to 10^6/sec at 340 GeV/c and for negative-beam intensities from 10^6/sec at 100 GeV/c to 3×10^5/sec at 280 GeV/c.

For beam momenta of 200 GeV/c or less, pions and kaons were identified by two differential Cerenkov counters. Positive beam particles at 340 GeV/c were taken to be purely protons; negative particles at 280 GeV/c to be purely pions.

For beam momenta of 200 GeV/c or less, all data were taken with the liquid hydrogen target in the standard position shown in Fig. 1. For positive 340-GeV/c and negative 280-GeV/c momentum beam, spectrometer-arm data were also taken at the standard target position. At these highest beam momenta calorimeter-arm data were taken with the target moved 1.04 m upstream to maintain the calorimeter acceptance at approximately 90 deg in the center-of-mass frame.

The target was a 5-cm-diameter, 30-cm-long flask filled with liquid hydrogen. The Mylar end caps of the flask were 0.13 mm thick. The windows of the vacuum enclosure were more than 14 cm

from the flask.

For calibration purposes a dipole magnet with adjustable azimuthal orientation was placed 10 m upstream of the target. By varying the orientation and magnetic field of the magnet, electrons and hadrons of known momentum could be directed over the entire face of the calorimeter. The dipole magnet was also used to direct beam particles into the spectrometer arm to check the spectrometer momentum calibration with the beam line calibration.

Both arms of the experiment were shielded from interactions which occurred far upstream of the target by concrete blocks placed adjacent to the beam pipe upstream of the rotating magnet. A wall of scintillation counters was placed about 2 m upstream of the hydrogen target to veto events accompanied by surviving charged particles from far-upstream interactions.

B. The Spectrometer Arm

A charged-particle spectrometer was formed by a single Fermilab BM109 magnet. The BM109 magnet has pole pieces which are 0.61 m wide by 1.83 m deep. The BM109 normally has a gap of 20.3 cm. Since the cross section for production of high-p_t particles is small we needed to make the acceptance of our spectrometer as large as possible. We therefore inserted 20.3-cm-thick steel spacers in the two flux return paths of the magnet; thus forming an expanded aperture which had the shape of a cross. Momentum analysis of tracks was restricted to the region of nearly uniform magnetic field in the central 0.61 m by 0.406 m aperture.

Measurements of the integrated field strength for paths passing normally through the magnet aperture were performed using a very long flip coil. The measurements were taken over a grid of positions which covered the full horizontal span and 2/3 of the vertical span of the central aperture. The measured variations (mostly less than 1%, approaching 10% very close to the horizontal edge) in magnetic field strength were taken into account in the momentum analysis.

The magnet was generally run at a magnetic field strength of 0.94 Tesla. The transverse momentum kick imparted to a particle traveling straight through the center of the aperture was 0.52 GeV/c.

The BM109 magnet straddled the beam line as shown in Fig. 1. The 20.3 cm gap between the coils produced by the insertion of the steel spacers provided a passageway for clean transmission of non-interacting beam particles through our apparatus. The magnet was oriented at an angle of 61 mrads with respect to the beam line so that the particles would enter the uniform field region at close to normal incidence. The entrance aperture of the magnet was 4.0 m from

the standard position of the target.

A high-p_t single-particle trigger was formed by three scintillation hodoscopes. One hodoscope, A, was placed upstream of the BM109 magnet at a distance of 3.66 m from the target; the remaining hodoscopes, B and C, were placed downstream of the magnet at distances of 6.88 m and 9.14 m respectively from the target.

The trigger hodoscopes were designed so that a minimum transverse momentum of 2 GeV/c could be required uniformly over the range, $39 < \theta < 132$ mrads , of production angles spanned by the A hodoscope. For each A element a range of bend angles was defined by a set of three adjacent B elements and four adjacent C elements. The maximum allowed bend angle was the same for both bend-away and bend-back tracks to achieve equal sensitivity to both negatively and positively charged particles. The elements were designed so that the range of bend angles for each A hodoscope element was proportional to the central production angle defined by that element. Thus lower-momentum particles were allowed at larger production angles such that the transverse momentum requirement was uniformly 2 GeV/c.

The transverse momentum threshold had a width due to the length of the target and the widths of the hodoscope elements. The threshold width depended on the production angle. For a production angle of 100 mrads the acceptance was 10% at 1.7 GeV/c and 90% at 2.75 GeV/c for trajectories which bend back to the beam line and was 10% at 1.6 GeV/c and 90% at 3.0 GeV/c for bend-away trajectories. The widths of the elements were made as narrow as feasible. There were 21 A elements, 23 B elements and 24 C elements. The A elements were the narrowest, ranging in width from 0.86 cm to 2.77 cm.

The vertical acceptance of the trigger was set by the 9.14 cm height of the A hodoscope elements. The B and C element heights were made slightly

oversize. At the exit of the magnet, the trigger trajectories filled 75% of the vertical span and nearly all of the horizontal span of the central aperture. The trigger acceptance was 0.70 steradian in the center-of-mass frame for a beam momentum of 200 GeV/c.

C. The Calorimeter Arm

A calorimeter was placed on the opposite side of the beam line from the spectrometer. The front face of the calorimeter was only 2.43 m from the standard position of the target. The calorimeter position was determined by our desire to have large acceptance in both arms of the experiment and by the necessity of fitting the calorimeter in front of the BM109 magnet.

The calorimeter was composed of two independent sections. The front section was designed to measure electromagnetic showers produced by entering gamma rays. This section was constructed of eight 0.64-cm-thick sheets of lead interleaved with 0.64-cm-thick sheets of plastic scintillator. The rear section was constructed of 32 2.54-cm-thick slabs of stainless steel interleaved with 0.64-cm-thick sheets of plastic scintillator. Each sheet of plastic scintillator consisted of a series of equal-width strips. The orientation of the strips was alternated between the horizontal and vertical directions at each successive depth in the calorimeter to give both x and y readout. In each section a sum over the longitudinal development of the shower was performed by adding the light from corresponding strips at the various depths. In effect, each section of the calorimeter was divided into horizontal and vertical segments as illustrated in Fig. 2.

The 0.52-m-wide by 1.02-m-high lead section was placed so that the nearest edge was 15 cm from the beam line. The aperture of the steel section at the mean shower depth was 0.59-m wide by 1.02-m high with the nearest edge 17 cm from the beam line. The acceptance of the lead section

was about 10% greater than the steel-section acceptance. The mean acceptance for a beam momentum of 200 GeV/c was 2.3 steredians.

The energy resolution of the calorimeter was measured to be $\sigma_E = 0.26\sqrt{E(\text{GeV})}$ for the lead section and $\sigma_E = 0.81\sqrt{E(\text{GeV})}$ for the steel section. The calorimeter and its measured response were described in more detail in our earlier report[4].

D. The Multiwire Chambers

Twenty-eight planes of multiwire chambers comprising a total of 18000 wires were used throughout both arms to measure the trajectories of charged particles. Seventeen of these planes were placed upstream of the BM109 magnet to measure the straight trajectories of particles emanating from the target. Eight of the upstream planes were centered on the beam line within 1.64 m of the standard target position to provide a good measurement of the position of the event vertex. Three upstream planes near the magnet aperture and six planes near the calorimeter provided good definition of the trajectories of the particles entering the two arms. Eleven planes placed downstream of the magnet were used to measure the exit trajectories from the spectrometer.

The planes were grouped into ten chambers. Two chambers were doublets of x and y-measuring planes. The other eight chambers were triplets of planes measuring a principal coordinate and coordinates at ±26.6 deg to this principal direction. The wire spacing was 2 mm for normally strung planes and was 1.8 mm for diagonally strung planes.

In the spectrometer arm the chambers were placed so that the principal direction was horizontal thus measuring the bend-plane projection of the trajectory with maximum precision. The two calorimeter arm chambers were placed with the priacipal direction vertical in order to span the large vertical acceptance of the calorimeter. The chamber arrangement is shown in Fig. 1.

The pattern of hit wires was read out in a two-stage process. The first stage was performed in parallel at each plane and consisted of coding and storing the addresses of the hit wires. In the coding process a pair of adjacent hit wires was given a single half-wire address corresponding to the midpoint between the two wires. For a sequence of four or more consecutive

hit wires only the half-wire addresses at the start and end of the sequence were coded. Upon the completion of the coding process the hit wire addresses from each plane were read out sequentially.

E. Chamber Performance and Spectrometer Resolution

Defining a particle to have been detected if a wire within a distance of two wire spacings from the point of passage records a hit, the chamber efficiencies were measured to be generally 97-98%. Two troublesome planes had measured efficiencies of about 90%. All 28 planes were in operation for all data reported in this paper.

With chamber efficiencies as measured the fractional error in momentum measured in the spectrometer was calculated to be $\sigma_p/p = 0.043\ [p(\text{GeV/c})/100]$. The fractional error in transverse momentum, σ_{p_t}/p_t, was largest at the smallest production angles. The increase in the fractional error was due not only to the decrease in the production angle but also to the increase of the momentum required to produce a given p_t value. The fractional transverse momentum error for p_t = 2 GeV/c at the smallest lab angle, 39 mrad, was calculated to be 2.1% for bend-back tracks and 2.3% for bend-away tracks.

IV. EVENT RECONSTRUCTION

A. The Spectrometer Arm

1. The Character of the Data

Analysis of the spectrometer-triggered data showed that only 1-2% of the events contained a genuine high-p_t trigger particle. In the design stage of the experiment calculations of the trigger rate were performed using a Monte Carlo simulation of multiparticle events. The trigger rate due to several-particle effects was calculated to be about ten times greater than the genuine single-particle rate. Our observed rate was another factor of 5 or 10 greater, probably due to effects of secondary interactions in the apparatus.

Our trigger had the effect of selecting the genuine high-p_t particle events as well as those events which produced enough secondary spray to satisfy the requirement falsely. Most events had a length of 300-400 16-bit words. The length distribution had a small tail which extended out to lengths of more than 800 words. The high-length tail posed a computing-time problem. No event with greater than 250 hits in the downstream chambers was analyzed. No analyzed event which yielded a genuine high-p_t particle had a downstream multiplicity greater than 175 hits; a strong indication that no genuine events were eliminated by the multiplicity cut.

Because of the complexity of many of the events the reconstruction algorithm was designed to require sufficient redundancy in the chamber information to guarantee that no false tracks were reconstructed. The algorithm required a minimum 10-constraint fit to the trigger trajectory. Most fits were over-constrained even more. A penalty in reconstruction efficiency was paid for this redundancy. The absolute reconstruction efficiency for

the spectrometer arm was estimated to vary within the range 60-90% over the course of the experiment. This estimate was corroborated by comparing (for 340-GeV/c pp reactions) our yield to the expected yield of pions, kaons, and protons based on measured cross sections [7]. A Monte Carlo model of the spectrometer arm was used in the calculation to account for the acceptance of our single-particle trigger. All results of the experiment which we report in this paper are not sensitive to the absolute efficiency of the spectrometer arm.

2. The Track Reconstruction Algorithm

The track reconstruction algorithm consisted of the following steps:

1) The trigger hodoscope hits were used to calculate a set of "reduced" triggers. A reduced trigger is a single A element matched with all valid B and C combinations present.

2) For each reduced trigger, a search for tracks was made in the downstream chambers over a region determined by the extreme B and C valid hits. A track was required to possess hits in at least eight of the eleven planes. The χ^2 distribution indicated that nearly all of the reconstructed tracks were genuine. Each track was projected back to the vertical midplane of the BM109 magnet. A cut (determined by the A element) requiring that the particle suffer only a small bend in passing through the magnet was then imposed. About 10% of the events survived the downstream analysis.

3) The position of the event vertex was calculated using the seventeen upstream planes. Judging by the sharpness with which the distribution of vertices defines the target length, the z-coordinate of the vertex is determined to better than 1 cm.

4) The point of origin of the upstream trajectory was fixed at the vertex. A search (over a region defined by the A element) for tracks was made in the two chambers closest to the magnet aperture. A track was required to possess hits in at least five of the six planes. The χ^2 distribution indicated that nearly

all of the reconstructed tracks were genuine.

5) The three-constraint fit at the magnet center was tested for each pair of upstream and downstream tracks. Surviving fits were checked to insure that the track passed through a valid combination of ABC hits..

6) The minimum χ^2 fit was taken to be the true track.

The limits of the various cuts were first calculated using the surveyed positions of the apparatus in the spectrometer arm and compensating for the expected resolution of the multiwire chambers. The program was then tested on a sample of events taken with the BM109 magnet current reduced to about 20% of its standard value. With the reduced current the nominal P_T trigger threshold was lowered to about 0.4 GeV/c; resulting in a sample of events which was mostly genuine single-particle triggers. The positions and limits of the cuts were tuned to insure full efficiency of the algorithm. Adjustments of less than 0.5 mm were required.

B. The Calorimeter Arm

The calorimeter measured the total energy carried by all entering particles as well as the x and y profiles of the energy distribution pattern. The lead section measured the energy carried by neutral pions; the steel section the energy carried by the remaining hadrons.

In our analysis we studied the distribution of the total momentum carried by all particles entering the calorimeter. We utilized an estimator (accurate in the small-angle approximation) of the total momentum which did not require the determination of the x and y coordinates and energy of each of the separate particles entering the calorimeter. The estimator used only the quantities: E, the total energy; $\langle x \rangle$ and $\langle y \rangle$, the mean position of the total energy; and σ_x and σ_y, the rms widths of the energy profiles. The total momentum was calculated by the following procedure:

(1) The rest masses of all entering particles were taken to be negligibly small.

(2) The masses of the groups of particles entering each calorimeter section were calculated by the approximate relation

$$\frac{m^2}{E^2} = 2 \left[\frac{\sigma_x^2 + \sigma_y^2}{z^2} \right]$$

where z is the distance along the beam line from the event vertex to the fiducial plane of the section (a plane at the depth where the shower maximum occurs on the average).

(3) The momentum of each group was then calculated by the relation

$$p = \sqrt{E^2 - m^2} \ .$$

For our events, m = 0.1 E so E and p differ by less than 1%.

(4) The direction of the momentum vector was taken to be along the line connecting the event vertex to the centroid (<x>, <y>) of the energy deposition pattern at the fiducial plane.

(5) The momentum vectors from the two calorimeter sections were added to obtain the total momentum vector for all particles entering the calorimeter.

The orientation of the momentum vector was expressed in terms of the azimuthal angle about the beam line

$$\phi_c = \tan^{-1}\left(\frac{<x>}{<y>}\right)$$

and the pseudorapidity along the beam line in the laboratory frame

$$\eta_c = -\ln\left(\tan\left(\frac{\theta}{2}\right)\right)$$

where θ is the laboratory polar angle.

V. EVENT DISTRIBUTIONS

The distributions of events obtained in the spectrometer-triggered mode of the experiment at the highest beam energies are now given. In this mode the experiment was sensitive to a flux of 2.6×10^9 280-GeV/c negative pions and to a flux of 0.41×10^9 protons striking the hydrogen target. Genuine high-p_t reaction samples of 9940 280-GeV/c π^-p events and 2418 340-GeV/c pp events were obtained.

The ratios of high-p_t particle production by the two different beams are shown in Table I. The ratios for both negative and positive particle production are given. The data have been summed over a range, $39 < \theta < 132$ mrads, of production angles which includes pieces of both beam and target regions. The absence of a negative charge in the initial pp state increasingly suppresses negative particle production at larger transverse momentum. The production ratios for positively charged particles are independent of transverse momentum and agree roughly with the ratio of the numbers of positive charges in the two initial states.

The variation of the charge-production ratio with production angle is shown in Table II. For the π^-p data, the +/- ratio systematically increases as the production angle increases from the π^- region to the p region. For the pp data, the +/- ratio is about 1.7 independently of the production angle. Our ratio agrees with measurements of pp reactions at 200 GeV/c [8]. The lack of variation with production angle reflects the forward-backward symmetry of the initial pp state.

The recoil response in the calorimeter arm for single high-p_T trigger particles in the spectrometer arm was the primary object of study in the analysis. On an event-by-event basis, wide variations (in response to trigger particles of similar transverse momentum) in the total transverse momentum in the calorimeter were observed. Nevertheless a clear correlation in the mean calorimeter response was seen.

The p_T measured in the calorimeter vs. the p_T of the spectrometer trigger particle is shown for 340 GeV/c pp reactions in Fig. 3 and for 280 GeV/c π^-p reactions in Fig. 4. The three low-p_T data points for the 280 GeV/c π^-p data were obtained from two runs taken with the BM109 current reduced to 20% of its usual value. For both 340 GeV/c pp and 280 GeV/c π^-p reactions the fractional rms width, $\sigma/\langle p_T \rangle$, of the distribution of measured transverse momenta in the calorimeter is 0.7 for 2.0-GeV/c-p_T spectrometer trigger particles and decreases gradually to 0.5 for 4.0-GeV/c-p_T trigger particles.

The azimuthal angle, ϕ_c, of the total momentum measured in the calorimeter vs. the azimuthal angle, ϕ_s, of the spectrometer trigger particle is shown for 340 GeV/c pp reactions in Fig. 5 and for 280 GeV/c π^-p reactions in Fig. 6. A tendency (which increases with p_T of the spectrometer trigger particle) towards coplanarity is clearly seen. For both 340 GeV/c pp and 280 GeV/c π^-p reactions the rms width of the ϕ_c distribution shows little variation with the p_T and ϕ_s of the trigger particle and is typically 0.3 rad.

The pseudorapidity, η_c, of the total momentum measured in the calorimeter vs. the pseudorapidity, η_s, of the spectrometer trigger particle is shown for 340 GeV/c pp reactions in Fig. 7 and for 280 GeV/c π^-p reactions in Fig. 8. For both 340 GeV/c pp and 280 GeV/c π^-p reactions no systematic variation of η_c with either the η_s or p_T of the trigger particle is observed. For a given η_s and p_T bin the rms width of the η_c distribution is typically 0.2. A change in η_c of 0.05 corresponds to a shift of 1.8 cm at the fiducial plane of the steel section of the calorimeter.

VI. ANALYSIS OF EVENT DISTRIBUTIONS

A. The Four-Jet Model

The analysis consisted primarily of comparisons of the experimental measurements to the predictions of a computer model of four-jet events. The four-jet model was phenomenological in nature. The model was equipped with several parameters. It was the object of the analysis to determine the range, if any, of values of these parameters which produces fits to our experimental measurements. The motivation for the four-jet model was the hope that reactions involving production of large (>2 GeV/c) transverse-momentum hadrons may be understood in terms of a single hard-scattering process among constituents of the two initial-state hadrons. The scattering process might result in the formation of an intermediate state which could be understood as consisting of four objects: the two scattered objects and the remainders of the two initial hadrons. The question of the identity of these objects was not addressed in our analysis. The objects will be referred to as quarks in all subsequent discussion. The masses of the quarks are always taken to be zero.

The final-state hadrons were generated by a two-step process. The first step was the generation of a four-quark intermediate state. Each quark was then independently transformed into a jet of hadrons to form the final state. The generation process was carried out in the center-of-mass frame of the initial-state hadrons.

The first two (toward and away) quarks generated represented the quarks which result from the hard scattering process. The transverse momenta of these quarks were constructed from two components: one component due to the momentum transfer in the scattering process, the other component due to the transverse momentum of the quark in the initial hadron. The probability that the toward quark received a transverse momentum, p_T, in the scattering process was parameterized as $d\sigma/dp_T^2 = e^{-2p_T/<p_T>}$. The probability that the toward quark possessed an initial transverse momentum, k_T, was parameterized as $dn/dk_T^2 = e^{-\pi k_T^2/4<k_T>^2}$. The values of $<p_T>$ and $<k_T>$ were adjusted in the analysis. The total transverse momentum of the toward quark was obtained by summing the p_T and k_T vectors with a random relative azimuthal orientation.

The distribution of longitudinal momentum, p_L, of the toward quark was based on measured p_L distributions for π^+ produced with transverse momentum between 1.0 and 2.5 GeV/c in pp collisions [7]. The generated distribution was of the form $dn/dy = f(x_L)$ where y is the rapidity of the quark, $x_L = p_L/p_0$, and p_0 is the maximum possible longitudinal momentum given the already determined transverse momentum of the quark. The function $f(x_L)$ was approximately $e^{-4.0x_L}$ for $0<x_L<.4$, fell as $e^{-7.7x_L}$ for $.4<x_L<.7$, and fell more steeply for larger x_L.

The longitudinal momentum of the away quark was generated so that

the longitudinal momentum of the toward-away two-quark system would be Gaussian-distributed. The two-quark longitudinal momentum distribution was expressed in terms of L, where L is the ratio of the two-quark longitudinal momentum to the maximum possible longitudinal momentum, $\sqrt{s}/2$. For pp reactions, the average value of L was taken to be zero. For πp reactions, <L> was adjusted in the analysis. The rms width, σ_L, of the two-quark longitudinal momentum distribution was not varied arbitrarily. Guidance as to a reasonable value of σ_L was obtained by folding quark longitudinal momentum distributions from each of the initial hadrons. In the folding process we imposed the requirement that the two-quark mass be large enough to produce our observed high-p_T trigger particles. The quark distribution for the proton was taken to be the sum of the distributions for each of the various quark flavors as deduced by Field and Feynman [1]. Similarly, the quark distribution for the pion was taken to be the sum of the Field-Feynman estimates for the various quark flavor distributions. The folding calculation gave the result $\sigma_L = 0.27$ for pp reactions and $\sigma_L = 0.34$ for πp reactions.

The next step was to generate the transverse momentum of the away quark. It was already determined that this quark had transverse momentum, $-p_T$, due to the hard scattering process. It remained to generate the transverse momentum that the away quark possesed in the initial hadron. It was always assumed that the toward and away quarks come from different hadrons. Consequently a k_T value for the remaining initial hadron was required to be generated. The k_T distribution was again taken to have the form $dn/dk_T^2 = e^{-\pi k_T^2/4<k_T>^2}$. In the

analysis $\langle k_T \rangle$ was always taken to have the same value in each initial hadron, irrespective of the identity of the beam hadron. The total transverse momentum of the away quark was then $-\underset{\sim}{p}_T + \underset{\sim}{k}_T$ where $\underset{\sim}{k}_T$ had a random orientation with respect to $-\underset{\sim}{p}_T$.

The last step was the generation of the beam and target quarks. The transverse momenta of these quarks were already determined by the left-over transverse momentum in the initial hadrons since the total transverse momentum of all quarks in each initial hadron must be zero. The longitudinal momenta of the beam and target quarks were calculated by the requirement that the energy-momentum four-vector of the four-quark state be the same as for the initial hadron state.

With the generation of the four-quark state completed, the final four-jet state was now generated. Each quark was independently transformed into a jet of hadrons. The jet generation procedure was designed so that the total energy of the jet particles would be equal to the total energy of the quark. The total momentum of the jet then must be less than the momentum of the zero-mass quark by an amount which depends on the jet mass which happens to be generated.

The longitudinal momenta of the jet particles were generated by a recursive technique. The generating distribution was $dn/dz = (1-z)^N$ where z is the ratio of the jet-particle longitudinal momentum to the energy in the parent quark system. The transverse momenta of the jet particles were generated according to the form $dn/dk_T^2 = e^{-k_T^2/2\sigma^2}$. The jet generation process began with the generation of the longitudinal momentum of the first jet particle with the parent quark possessing its full energy as assigned in the generation of the four-quark state. The

transverse momentum of the first jet particle relative to the quark axis was then generated. The particle mass was taken to be the pion mass. The total energy of the jet particle was then subtracted from the energy of the quark system, yielding a value of energy to be used in the generation of the longitudinal momentum of the next jet particle. The generation of jet particles proceeded in this fashion until the energy in the quark system fell below a preset value of 0.2 GeV.

In the development of the model, the values of the parameters N and σ were adjusted until the generated jets resembled the jets of hadrons produced in e^+e^- annihilations as observed at the DORIS and PETRA storage rings. The results [9] of the PLUTO collaboration for the average transverse and average longitudinal momenta of the jet particles are reproduced in Fig. 9. In order to fit the data, the values of both σ and N were required to vary with the total jet energy. The value of N was 2 for zero-energy jets and gradually increased to 3.2 for 14-GeV-energy jets. The value of σ was 0.26 GeV/c at zero energy and increased to 0.42 GeV/c at 14 GeV. A further requirement imposed was that the angular distrubution for all particles generated for two back-to-back jets be smooth in passing from the forward to the backward hemisphere. This smoothness criterion required that the transverse momenta be scaled down (by an average factor of 0.75) for jet particles with center-of-mass longitudinal momenta less than 1 GeV/c in magnitude. The behavior of the computer model is represented by the solid lines in Fig. 9.

B. The Mode of the Experimental Apparatus

The principal features of the spectrometer arm model were the three trigger hodoscopes and the magnetic field of the BM109 magnet. The hodoscopes were modeled simply as two-dimensional apertures. The magnetic field was modeled as being limited to the volume between the magnet pole pieces. The field strength was taken to be independent of the longitudinal position within the magnet. The appropriate transverse variation of the field was then calculated from the results of the long-flip-coil measurements made in the magnet calibration process.

The curved trajectories of charged particles in the magnetic field were calculated by breaking the field region into ten equal-length longitudinal segments. Each longitudinal segment was then approximated as a thin lens.

The response of the multiwire chambers was calculated for particles which were found to satisfy the hodoscope trigger requirement. Approximations to the reconstructed tracks upstream and downstream of the BM109 magnet were calculated by generating errors in the true positions of the wire triplets according to the calculated resolution (σ_y = .35 mm, σ_x = .92 mm) of a fully efficient triplet. The reconstructed downstream trajectory was calculated from the modified positions in the triplets in the two chambers that provided the maximum lever arm for this track. The reconstructed upstream trajectory was calculated using the generated vertex and the modified

position of the wire triplet in the chamber located at the entrance to the BM109 magnet.

The spectrometer arm model was not made more elaborate since the primary object of the analysis was not to measure precisely inclusive production cross sections for high-pt single particles but to measure the recoil response in the calorimeter once a high-pt particle is detected in the spectrometer arm. The spectrometer arm model is then not critical.

The calorimeter-arm model was based closely on the response of the calorimeter as measured in the calibration process. The calorimeter sums over the longitudinal development of the shower so the calibration data consisted of sets of x and y profiles of deposited energy for electrons and hadrons of known momentum. Most of the calibration data were taken at a momentum of 20 GeV/c. Particles which entered the calorimeter near its center were used to determine the lateral spreading of the hadron showers. For 20-GeV/c hadrons the projected rms width was measured to be 7.5 cm. The rms width of the width distribution was 3.1 cm. An "average" profile (for use in the model) was constructed by summing all the patterns. The lateral spreading was found to be independent of the energy response. The lateral spreading of the electromagnetic showers was too small to be measured accurately in our calorimeter.

The lead and steel sections of the calorimeter were modeled independently. Each section was modeled in terms of a fiducial plane at the average depth of the shower maxima. The longitudinally summed energy-deposition patterns measured in the calibration process were

taken to occur solely at the position of this plane.

The algorithm for calculating the response of the steel section to an entering hadron was: (1) An energy was drawn from a distribution based on the measured energy response for particles entering near the center of the calorimeter. This energy was divided equally between the x-measuring and y-measuring counters. (2) Independent widths for the x and y profiles were drawn from the measured width distribution. (3) The x and y profiles were obtained by scaling the average profile to these widths. (4) The energy distribution in the calorimeter was then calculated by centering the profiles on the position of the incident hadron at the fiducial plane. The fraction of energy in the x-measuring counters lying within the y-boundaries of the calorimeter was calculated using the y-profile. The surviving energy was then alloted among the x-measuring counters using the x-profile. Energy in the x-profile beyond the x-boundaries of the calorimeter was discarded. A similar process was carried out for the y-measuring counters. In this fashion the necessary modification of the response at the edges and corners of the calorimeter was accomplished. The response algorithm successfully reproduced the response for hadrons incident near the edge of the calorimeter as measured in the calibration process.

A similar algorithm was used to calculate the response of the lead section to gamma rays arising from the decays of neutral pions. The response to gamma rays was taken to be the same as the measured response to electrons. All electromagnetic showers were taken to have the same profile. The shape of the profile was obtained by requiring that the calculated response at the edges reproduce our

(poorly) measured edge response. The profile adopted was sharply peaked at its center and had an rms width of 1.2 cm.

C. Comparison of the Four-Jet Model to the Data

We considered our measurement of the calorimeter response to high-p_T trigger particles in the spectrometer to be the most decisive test of our model's fundamental assumption of a single hard-scattering process. In the variation of the parameters of the model we directed our attention first to the two-arm correlation data. Once values of the parameters had been determined by the two-arm data we merely verified that the predictions of the model were in reasonable agreement with the inclusive data from each of the two arms. The value of the parameter $\langle p_T \rangle$ has no direct effect on the two-arm correlation predictions hence was considered to be of secondary importance.

We began our comparison with the 340-GeV/c pp data. Since the symmetry of the initial state forces $\langle L \rangle$ to be zero we had only two free parameters in our model. We set $\langle k_T \rangle$ to be 0.3 GeV/c and found that a value of 0.95 GeV/c for $\langle p_T \rangle$ produced a good fit to the slope of the measured inclusive yield [4] in our calorimeter. With $\langle p_T \rangle = 0.95$ GeV/c we proceeded to test the model for the spectrometer-arm trigger mode of the experiment. The predicted yield of trigger particles with $p_T > 2.5$ GeV/c was $dn/dp_T = e^{-2.45p_T}$. Our observed yield was $dn/dp_T = e^{-2.6p_T}$. With this level of agreement we proceeded to vary the parameter $\langle k_T \rangle$. We were forced to increase the value of $\langle k_T \rangle$ to 0.9 GeV/c before fair agreement (see Fig. 3) with the observed p_T response in the calorimeter could be obtained. However, even at this elevated value of $\langle k_T \rangle$, the model predicted (see Fig. 5) a greater degree of coplanarity than was observed in our data. The predictions for the pseudorapidity correlation are compared to the data in Fig. 7. In the model, the generation of a more-forward toward quark results in the generation of a more-backward away quark in order to meet the specifications for the $\langle L \rangle$ distribution. Thus we expect, at sufficiently high p_T, that η_c will be predicted to decrease as η_s increases. The results of our calculation show that this effect is barely discernible for the trigger-particle transverse momenta we have available in our experiment. Our pseudorapidity data does not definitely discriminate between the two choices of $\langle k_T \rangle$ values. The slope of the η_c-vs.-η_s correlation is less sensitive to errors in the calorimeter calibration than is the absolute value of η_c. On the basis of this slope, the data show a preference for $\langle k_T \rangle = 0.9$ GeV/c. The predictions for the inclusive distributions in each arm were essentially unchanged by the increase of $\langle k_T \rangle$ to 0.9 GeV/c and remained in fair agreement with our data.

We next compared our four-jet model to the 280-GeV/c $\pi^- p$ data. We left the parameter $\langle p_T \rangle$ set to the value 0.95 GeV/c. Three choices of values for the remaining pair of free parameters were made: (1) $\langle k_T \rangle = 0.3$ GeV/c, $\langle L \rangle = 0.1$; (2) $\langle k_T \rangle = 0.9$ GeV/c, $\langle L \rangle = 0.$; (3) $\langle k_T \rangle = 0.9$ GeV/c, $\langle L \rangle = 0.1$. For these three choices the predictions for the yield of trigger particles with $p_T > 2.5$ GeV/c varied from $dn/dp_T = e^{-2.5p_T}$ to $dn/dp_T = e^{-2.7p_T}$, all in reasonable agreement with our measured yield of $dn/dp_T = e^{-2.65p_T}$. The predictions for the p_T response in the calorimeter are compared to the data in Fig. 4. Similarly we compare the predictions for the degree of coplanarity to the data in Fig. 6 and the predictions for the pseudorapidity correlation to the data in Fig. 8. In these three comparisons we include predictions even at low values of trigger-particle p_T where the assumptions of the model are not expected to be accurate. In all cases we find that the best agreement with our data is obtained with choice (3) for the parameter values.

The calorimeter acceptance (see Fig. 2) is centered slightly backward in the center-of-mass frame for 280-GeV/c π^-p reactions. In azimuth, the calorimeter acceptance is centered opposite to the spectrometer acceptance. By increasing $\langle L \rangle$, we sweep on average more and more of the away jet (which is recoiling from the toward jet that provided the spectrometer trigger particle) forward past our calorimeter acceptance. Similarly, by increasing $\langle k_T \rangle$, we disperse the away jets and thereby reduce the calorimeter acceptance for these jets on the average. With less of the away jet detected, the contribution of particles from the target and (less importantly) beam jets has more of an effect on the total response of the calorimeter. Our model calculations clearly show how the expected four-jet correlation effects are diminished by increasing $\langle k_T \rangle$ and $\langle L \rangle$.

Since increasing either $\langle k_T \rangle$ or $\langle L \rangle$ has the same type of effect, we expect that a family of $\langle k_T \rangle$, $\langle L \rangle$ pairs which produce fits to our 280-GeV/c π^-p data could be mapped out. We have determined one point on this curve. Our π^-p measurements seem to be unable to provide separate determinations of $\langle k_T \rangle$ and $\langle L \rangle$ on their own. In the 340-GeV/c pp data, where we had no freedom to vary $\langle L \rangle$, we determined that $\langle k_T \rangle = 0.9$ GeV/c. If we adopt this value for πp reactions as well, we then determine that $\langle L \rangle = 0.1$.

We expect that $\langle L \rangle$ should be greater than zero for π^-p reactions due to the slower fall-off with x of the quark distribution function for the π^- as compared to the quark distribution function for the proton. It is difficult to quantify this expectation. We have measured the average longitudinal momentum of two-quark systems which suffer hard collisions and subsequently produce a trigger-hadron for our apparatus. Our result is linked to the quark distributions

in the initial hadrons through the quark scattering dynamics. This link is made less distinct by the effects of the apparently large initial transverse momentum of the quarks.

With the information available in our experiment we limit ourselves to the following remark. By folding together the Field-Feynman quark distributions for the pion and proton (with no initial transverse momenta) while imposing the requirement that the two-quark mass be large enough to produce a final-state hadron with transverse momentum greater than a threshold value, p_T, we obtain the results: $p_T = 0.6$ GeV/c, $\langle L \rangle = 0.04$; $p_T = 1.7$ GeV/c, $\langle L \rangle = 0.10$; $p_T = 2.9$ GeV/c, $\langle L \rangle = 0.21$; and $p_T = 4.1$ GeV/c, $\langle L \rangle = 0.27$. Our result that $\langle L \rangle = 0.1$ indicates that the two-quark mass threshold required to produce our trigger-hadrons is considerly reduced by the large transverse momenta of the quarks in the initial hadrons.

The validity of the four-jet model would be most convincingly demonstrated by successfully fitting, with the same choice of parameter values, the data over a wide range of trigger-particle transverse momenta. In our π^-p sample we have significant numbers of events for trigger-particle transverse momenta in the range $1.5 < p_T < 3.5$ GeV/c. For the lower half of this range our model (with choice (3)) predicts slightly greater calorimeter transverse-momentum values and a slightly greater coplanarity signal than we observe in our data. For the upper-half range our model gives a good fit (although the ϕ_c values in Fig. 6(d) are slightly low the ϕ_c-vs.-ϕ_s slope is accurately fit) to the data. Thus we see that we have not achieved a p_T-independent fit. Since it would require even greater values of $\langle k_T \rangle$ and $\langle L \rangle$ to fit the data in the lower-half range we judge that the accuracy of our model increases with p_T over the range of trigger-particle transverse momenta available in our data.

D. Comparison with Other Experiments

The UA2 experiment at the CERN collider has seen [10] clear examples of four-jet topologies in large-transverse-energy ($E_T > 60$ GeV) $p\bar{p}$ events at $\sqrt{s} = 540$ GeV. Also at the CERN collider, the UA1 experiment [11] has observed rapidity and azimuthal angle correlations between high-p_T charged particles which suggest coplanar production of two clusters in opposite azimuthal hemispheres.

Four-jet topologies have been seen to be much less distinct at lower values of $\sqrt{s}$. As a consequence these lower-energy experiments have had to cope with a selection problem. Each experiment picks out the subset of large-transverse-energy events which happens to satisfy its trigger requirements. The extent to which four-jet events are present in this sample must than be determined through comparison of the data to the predictions of a computer model of four-jet events.

At the CERN ISR, the Axial Field Spectrometer Collaboration [12] has measured pp reactions at $\sqrt{s}$ =63 GeV in a large-aperture spectrometer which was triggered on the transverse energy in a 1.7-sr-acceptance hadron calorimeter. By comparing their data to the predictions of the ISAJET four-jet model [13] with and without a hard-scattering component they deduce that the hard component dominates in events in which the trigger E_T exceeds 10 GeV.

Also at the CERN ISR, The CCOR Collaboration has measured pp reactions at $31<\sqrt{s}<62$ GeV using a large-acceptance spectrometer triggered on high-p_T neutral pions in a limited-azimuth array of lead glass counters. From measurements, for all charged particles in the event, of the component of the transverse momentum which is out of the plane formed by the trigger π^0 and the intersecting beams, the CCOR group was able to deduce [14] mean values for the parton transverse momentum k_T in the initial-state protons. The value of $\langle k_T^2 \rangle^{1/2}$ was determined to increase slowly with both the trigger-particle transverse momentum, p_{Trig}, and $\sqrt{s}$. In the kinematic region ($\sqrt{s}$ = 31 GeV, p_{Trig} = 3.2 GeV/c) which is quite close to our experiment, the CCOR result was $\langle k_T^2 \rangle^{1/2} = 0.8$ GeV/c. This result is slightly less than our result $\langle k_T^2 \rangle^{1/2} = 2\langle k_T \rangle/\sqrt{\pi} = 1.0$ GeV/c obtained by analyzing the correlation of all hadrons recoiling from a single high-p_T charged pion.

Fixed-target experiments at CERN (πp and pp collisions at $\sqrt{s}$ = 23 GeV) and at Fermilab (pp collisions at $\sqrt{s}$ = 27 GeV) which triggered on the total transverse energy in full-azimuthal-acceptance calorimeters have observed [5,6] that planar events constitute only a small fraction of the event sample. Furthermore this fraction is observed not to increase for E_T values which extend out to 20 GeV.

Fermilab E260 has measured event structure in πp and pp reactions at $\sqrt{s}$ = 19 GeV using a multiparticle spectrometer triggered on hadron calorimeters of limited azimuthal acceptance. The observed event structure (on both the trigger and away sides) was explained [3] in terms of a QCD four-jet model which included the effects of both quark and gluon two-body scattering.

Fermilab E395 [2] measured the correlation between groups of hadrons which enter two calorimeter arms of limited azimuthal acceptance. The measurements were made for πp reactions at $\sqrt{s}$ = 19 GeV and pp reactions at $\sqrt{s}$ = 19-27 GeV. By comparing the correlated angular distributions in the two arms for πp and pp reactions, E395 was able to show that the πp reactions are more forward than the pp reactions on average. Their result agrees qualitatively with our result that $\langle L \rangle = 0.1$ for πp reactions. By ascribing the imbalance in transverse momentum in the two arms to parton transverse momentum effects, values of $\langle k_T^2 \rangle^{1/2}$ were determined. The value of $\langle k_T^2 \rangle^{1/2}$ was observed to be large and to increase slowly with the average transverse momentum, p_{TA}, in the two calorimeters. The value of $\langle k_T^2 \rangle^{1/2}$ was observed to increase from 0.9 GeV/c at p_{TA} = 2.3 GeV/c to 1.3 GeV/c

at $p_{TA} = 4.1$ GeV/c. This result corresponds closely to our result that $\langle k_T^2 \rangle^{1/2} = 1.0$ GeV/c. As in our experiment, E395 could see no apparent difference in $\langle k_T^2 \rangle^{1/2}$ for πp and pp reactions.

VII. SUMMARY

We have measured high-p_T correlations in 340-GeV/c pp and 280-GeV/c $\pi^- p$ reactions. Correlations between single high-p_T trigger particles on one side of the beam line and groups of particles entering a calorimeter on the opposite side of the beam line were measured. On an event-by-event basis we observe, in response to similar-p_T trigger particles, wide variations in the total calorimeter response. Nevertheless a clear correlation is seen after averaging over many events. We see, as the trigger-particle transverse momentum increases, an increasing transverse momentum in the calorimeter as well as an increasing degree of coplanarity with the trigger particle of the total calorimeter response.

We have developed a phenomenological four-jet model and compared the predictions of this model to our data. In the model we assume that high-p_T reactions proceed via a single hard-scattering process among the hadron constituents. The subsequent hadronization of the scattered constituents is taken to be the same as the hadronization measured in e^+e^- reactions. We find that our data can be fit by the model only if we give large (0.9 GeV/c) transverse momenta to the constituents of the initial hadrons. We present evidence that the high-p_T component of $\pi^- p$ reactions is forward on average in the $\pi^- p$ center-of-mass frame.

ACKNOWLEDGEMENTS

We thank K. Turner for her valuable assistance in setting up the multiwire chamber readout system and P. McManus for his design of this system. We thank R. Krull for his work in constructing the calorimeter. The work of M. Delay and R. Sjoberg on the on-line program is gratefully acknowledged. We thank J. Rutherfoord for his assistance during the data-taking and Lisa Chen, M.J. Fox, and J. Hanson for their work on off-line programming.

This work was performed at Fermilab, which is operated by Universities Research Association, Inc., under contract with the U.S. Department of Energy. The assistance of the Meson Lab staff and the use of the Fermilab computing facilities are gratefully acknowledged. This work was supported in part by the National Science Foundation.

REFERENCES

[1] S.D. Ellis and M.B. Kislinger, Phys. Rev. D9(1974)2027;
R.D. Field and R.P. Feynman, Phys. Rev. D15(1976)2590.

[2] M.D. Corcoran et al., Phys. Rev. Lett. 41(1978)9;
M.D. Corcoran et al., Phys. Rev. D21(1980)641;
M.D. Corcoran et al., Phys. Lett. 44(1980)514.

[3] C. Bromberg et al., Nucl. Phys. B171(1980)1.

[4] V. Cook et al., Nucl. Phys. B186(1981)219.

[5] C. DeMarzo et al., Phys. Lett. 112B(1982)173.

[6] B. Brown et al., Phys. Rev. Lett. 49(1982)711.

[7] B. Alper et al., Nucl. Phys. B100(1975)237.

[8] C. Bromberg et al., Phys. Rev. Lett. 43(1979)561.

[9] PLUTO Collaboration, Ch. Berger et al., Phys. Lett. 78B(1978)176;
PLUTO Collaboration, Ch. Berger et al., Phys. Lett. 86B(1979)418.

[10] UA2 Collaboration, M. Banner et al., Phys. Lett. 118B(1982)203.

[11] UA1 Collaboration, G. Arnison et al., Phys. Lett. 118B(1982)173.

[12] Axial Field Spectrometer Collaboration, T. Åkesson et al.,
Phys. Lett. 118B(1982)185.

Axial Field Spectrometer Collaboration, T. Akesson et al.,
Phys. Lett. 118B(1982)193.

[13] F.E. Paige and S.D. Protopopescu, ISAJET: A Monte Carlo Generator for pp and $\bar{p}p$ Interactions, Brookhaven National Laboratory report BNL-29777(1980).

[14] CCOR Collaboration, A.L.S. Angelis et al., Phys. Lett. 97B(1980)163.

Table I. The charged-particle production ratio of 280 GeV/c π^-p and 340 GeV/c pp reactions vs. transverse momentum. The ratios are given for both negatively and positively charged particles. The data have been summed over production angles $39 < \theta < 132$ mrads.

p_T INTERVAL (GeV/c)	1.5 - 2.0	2.0 - 2.5	2.5 - 3.0
$\frac{280\text{-GeV/c } \pi^-p \to h^-}{340\text{-GeV/c } pp \to h^-}$	.89 ± .045	.97 ± .065	1.42 ± .23
$\frac{280\text{-GeV/c } \pi^-p \to h^+}{340\text{-GeV/c } pp \to h^+}$	.49 ± .02	.51 ± .03	.48 ± .04

Table II. The charge production ratio vs. production angle for a range of transverse momenta. The ratios are given for both 280 GeV/c π^-p and 340 GeV/c pp reactions. The production angles in the center-of-mass system were calculated assuming zero-mass particles.

	+/- for 280-GeV/c π^-p			+/- for 340-GeV/c pp		
lab angle (rad)	.039-.055	.055-.078	.078-.132	.039-.055	.055-.078	.078-.132
c.m. angle (deg)	51-68	68-88	88-117	55-73	73-93	93-122
p_T Interval (GeV/c)						
1.5 - 2.0	.87 ± .035	.99 ± .05	1.13 ± .07	1.79 ± .15	1.50 ± .16	1.95 ± .24
2.0 - 2.5	.72 ± .05	.90 ± .06	1.21 ± .10	1.71 ± .20	1.78 ± .25	1.44 ± .23
2.5 - 3.0	.99 ± .12	.76 ± .11	1.20 ± .18			
3.0 - 3.5	.68 ± .15	.74 ± .20	1.48 ± .30			

FIGURE CAPTIONS

Fig. 1. Plan view of the experiment.

Fig. 2. Beam view of the experiment. The polar angles for the center-of-mass frame of a 280-GeV/c π^-p reaction are superposed.

Fig. 3. The response in the calorimeter arm to high-p_T single-particle triggers in the spectrometer arm for 340-GeV/c pp reactions. The solid lines are predictions of the four-jet model.

Fig. 4. The response in the calorimeter arm to high-p_T single-particle triggers in the spectrometer arm for 280-GeV/c π^-p reactions. Shown also are three low-p_T data points taken in special runs with reduced magnet current. The solid lines are predictions of the four-jet model.

Fig. 5. The mean azimuthal angle of the transverse momentum measured in the calorimeter versus the azimuthal angle of the trigger particle in the spectrometer for 340-GeV/c reactions. Equal values of ϕ_c and ϕ_s correspond to a coplanar response. Note the expanded vertical scale. The data are for trigger-particle transverse momenta in the range $1.5<p_T<2.5$ GeV/c. The solid lines are predictions of the four-jet model.

Fig. 6. The mean azimuthal angle of the transverse momentum measured in the calorimeter versus the azimuthal angle of the trigger particle in the spectrometer for 280-GeV/c π^-p reactions. The data are shown for four bins of trigger-particle transverse momentum. The solid lines are predictions of the four-jet model.

Fig. 7. The mean pseudorapidity of the total momentum measured in the calorimeter versus the pseudorapidity of the trigger particle in the spectrometer for 340-GeV/c pp reactions. The pseudorapidities are calculated in the laboratory frame. Note the expanded vertical scale. The solid lines are predictions of the four-jet model. The data are shown for two bins of trigger-particle transverse momentum.

Fig. 8. The mean pseudorapidity of the total momentum measured in the calorimeter versus the pseudorapidity of the trigger particle in the spectrometer for 280-GeV/c π^-p reactions. The data are shown for four bins of trigger-particle transverse momentum. The solid lines are predictions of the four-jet model.

Fig. 9. The mean longitudinal and transverse momenta of the particles in a jet as generated by the Monte Carlo model. The model was developed to reproduce the measured hadronization in e^+e^- reactions at the corresponding energy. In the figure we have reproduced the data of the PLUTO Collaboration taken at the DORIS and PETRA storage rings [9].

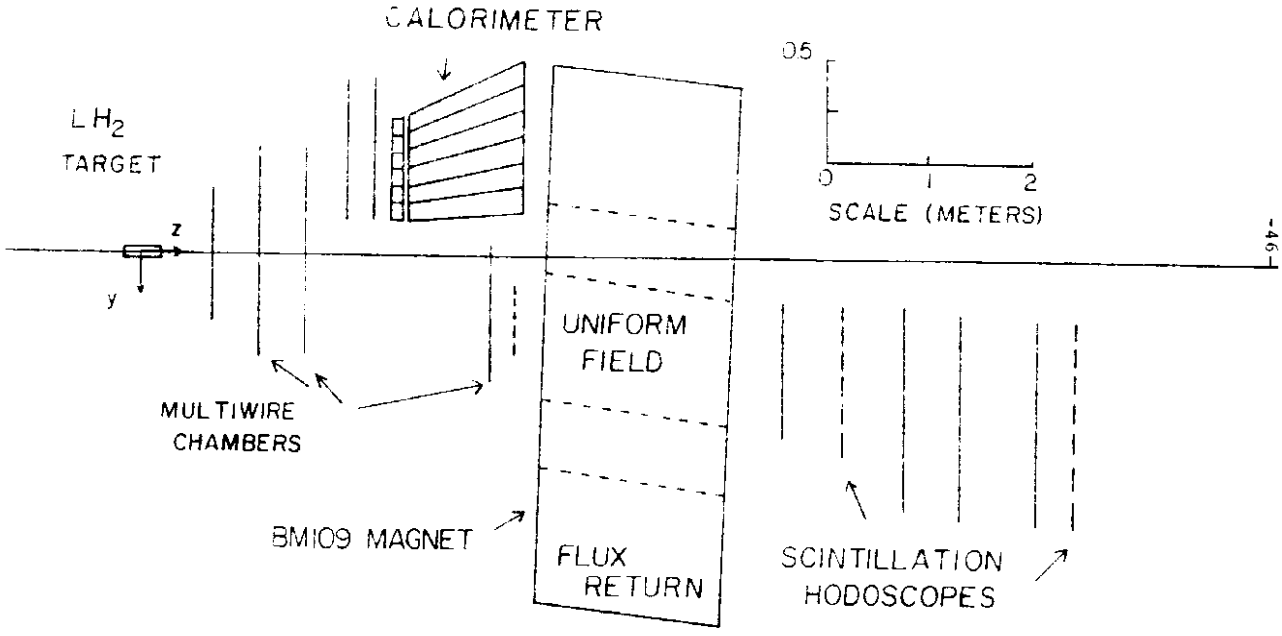
CALORIMETER
LH2
TARGET
z
y
MULTIWIRE
CHAMBERS
BM109 MAGNET
UNIFORM
FIELD
FLUX
RETURN
SCINTILLATION
HODOSCOPES
0
1
2
SCALE (METERS)

Fig. 1.

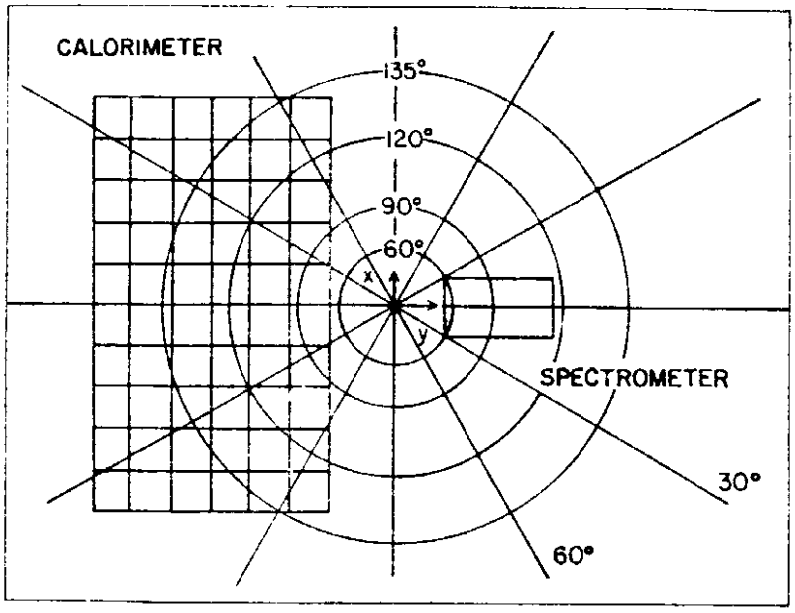
CALORIMETER
135°
120°
90°
60°
x
y
SPECTROMETER
30°
60°

Fig. 2.

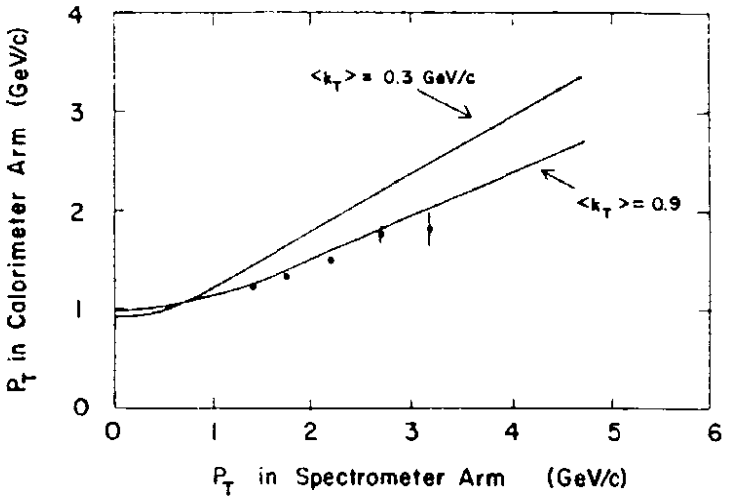
P_T in Calorimeter Arm (GeV/c)
P_T in Spectrometer Arm (GeV/c)
$\langle k_T \rangle$ = 0.3 GeV/c
$\langle k_T \rangle$ = 0.9
0
1
2
3
4
5
6

Fig. 3.

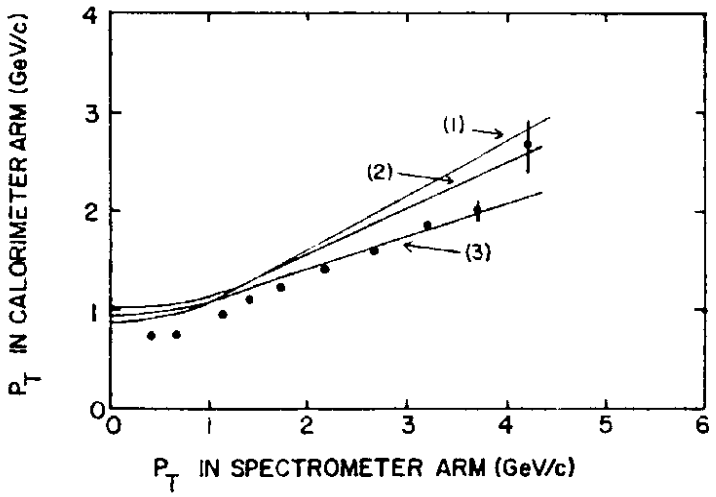
P_T IN CALORIMETER ARM (GeV/c)
P_T IN SPECTROMETER ARM (GeV/c)
(1)
(2)
(3)
0
1
2
3
4
5
6

Fig. 4.

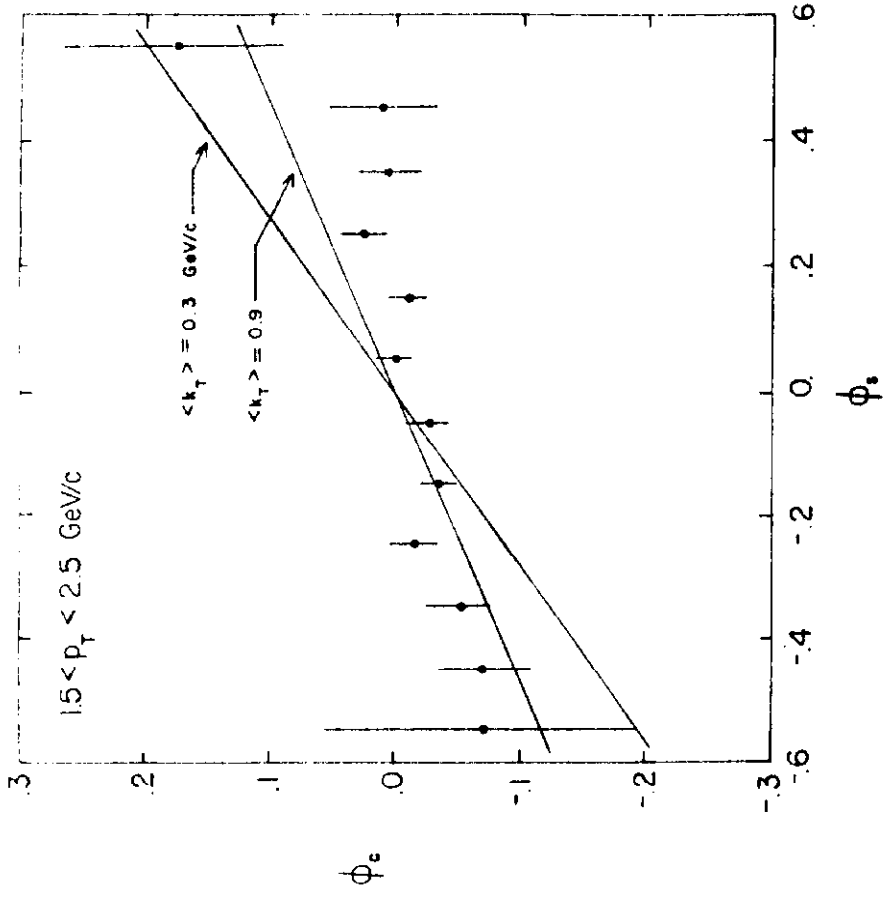
1.5 < p_T < 2.5 GeV/c
<k_T> = 0.3 GeV/c
<k_T> = 0.9
ϕ_c
ϕ_s

Fig. 5.

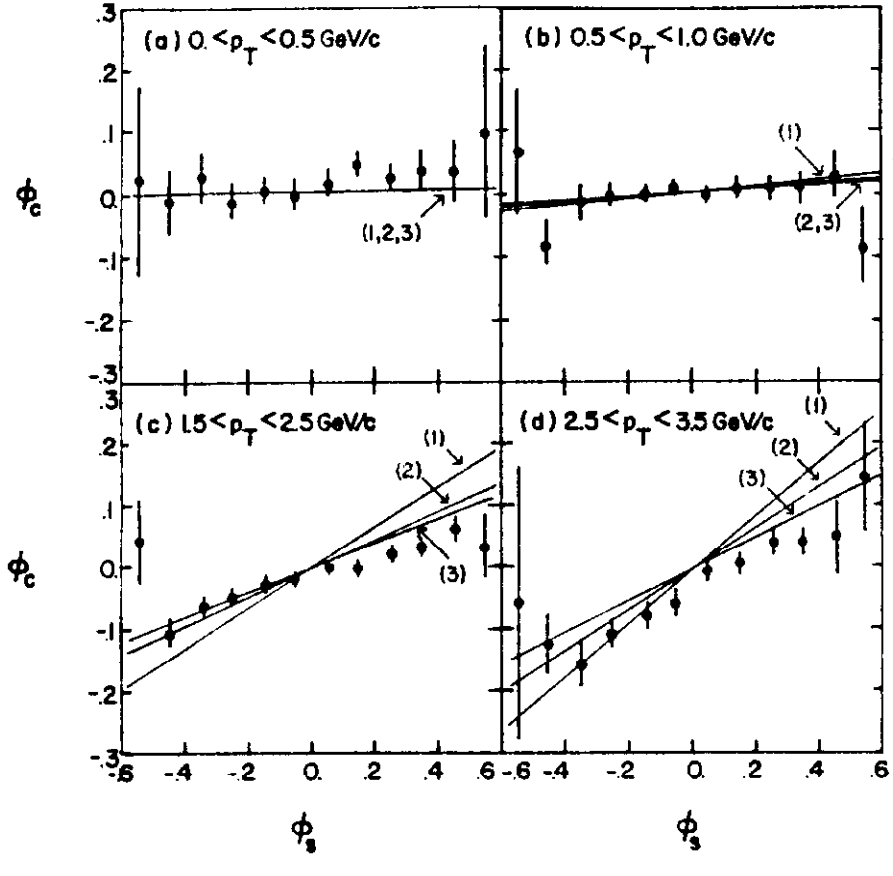
(a) 0. < p_T < 0.5 GeV/c
(b) 0.5 < p_T < 1.0 GeV/c
(c) 1.5 < p_T < 2.5 GeV/c
(d) 2.5 < p_T < 3.5 GeV/c
(1,2,3)
(2,3)
(1)
(2)
(3)
ϕ_c
ϕ_s

Fig. 6.

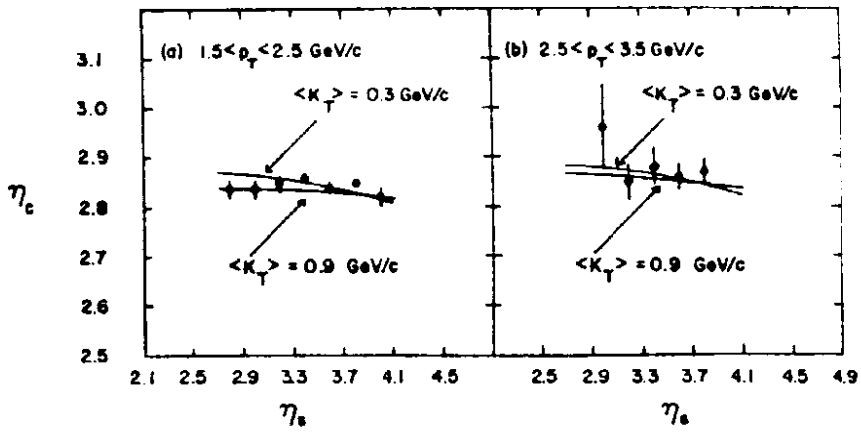
(a) 1.5<p_T<2.5 GeV/c
(b) 2.5<p_T<3.5 GeV/c
<K_T> = 0.3 GeV/c
<K_T> = 0.9 GeV/c
η_c
η_s

Fig. 7.

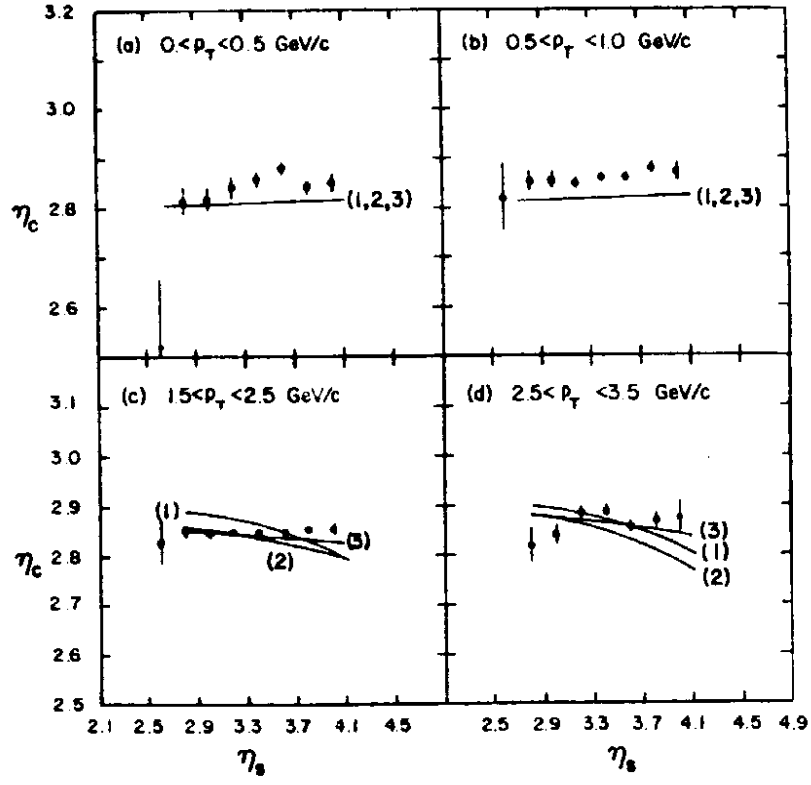
(a) 0<p_T<0.5 GeV/c
(b) 0.5<p_T<1.0 GeV/c
(c) 1.5<p_T<2.5 GeV/c
(d) 2.5<p_T<3.5 GeV/c
(1,2,3)
(1)
(2)
(3)
η_c
η_s

Fig. 8.

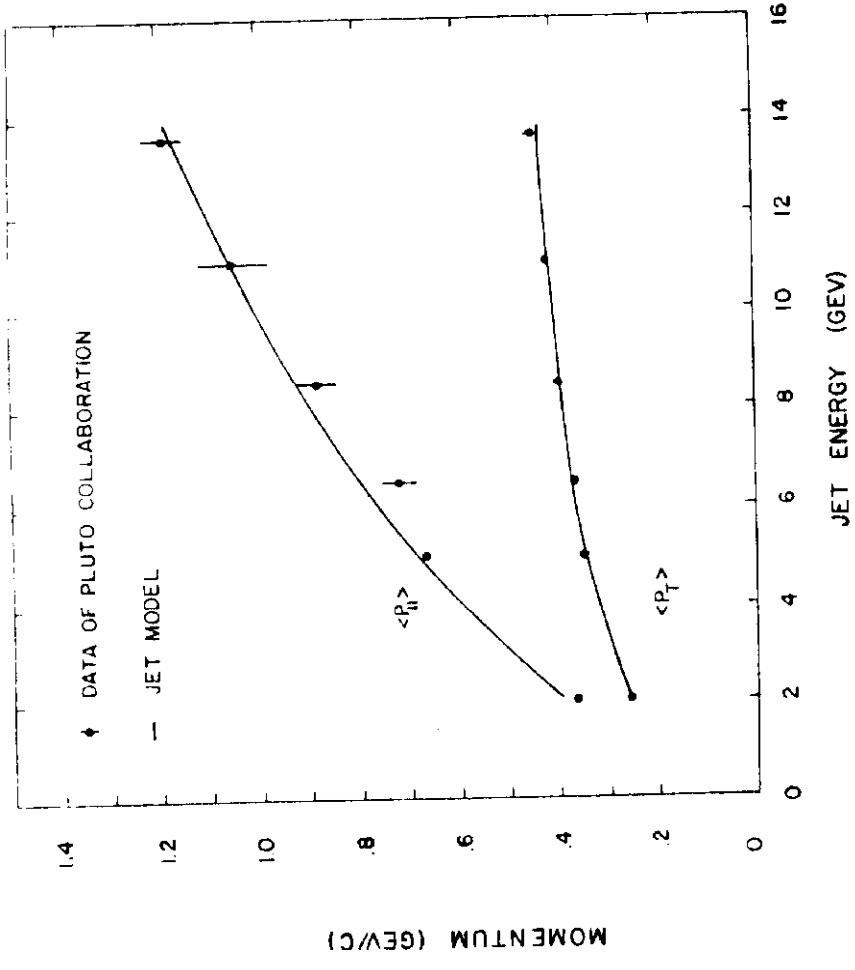
DATA OF PLUTO COLLABORATION
JET MODEL
$\langle P_{\parallel} \rangle$
$\langle P_{\perp} \rangle$
MOMENTUM (GEV/C)
JET ENERGY (GEV)
0
.2
.4
.6
.8
1.0
1.2
1.4
0
2
4
6
8
10
12
14
16

Fig. 9.